



Norwegian University of
Science and Technology

Numerical Modelling of Wave Interaction with Floating structures and Moored Floating Structures

Tural Mammadov

Coastal and Marine Engineering and Management

Submission date: July 2018

Supervisor: Hans Sebastian Bihs, IBM

Norwegian University of Science and Technology
Department of Civil and Environmental Engineering



| | | | | |
|--|--|---|--------------|--|
| Report Title: Numerical Modelling of Wave Interaction with Floating Structures and Moored Floating Structures | Date:06/07/2018 | | | |
| | Number of pages (incl. appendices): 41 | | | |
| | Master Thesis | X | Project Work | |
| Name: Tural Mammadov | | | | |
| Professor in charge/supervisor: Hans Bihs | | | | |
| Other external professional contacts/supervisors: Arun Kamath, Tobias Martin | | | | |

| |
|---|
| <p>Abstract:</p> <p>The thesis was focused on the validation of numerical data for floating bodies as well as moored-floating bodies in waves using experimental data and a systematic investigation of the influence of different mooring systems on the motion of floating bodies. For this purpose, the focus of the thesis work was concentrated on the motion of a free-floating body using the CFD model REEF3D. After the validation of results obtained numerically for heave decay test for the cylinder with the finest mesh size, the goal was to apply this data on the free-floating barge with more complex 3DOF motion. In addition, different diameter cylinder sizes were analysed to observe and study changes in behaviour graphically. After that, the mooring system was employed for the stabilization of the cylinder at one point. Obtained results were also used in the 3DOF floating barge.</p> <p>The floating barge 3DOF motion was analysed and compared with experimental data. Numerically obtained results had convergence with experimental ones. In addition, mooring analyses were performed also for this case. Mooring system parameters used for 3DOF floating barge were the ones obtained and analysed from cylinder case. Finally, the 6DOF motion of a 3D moored-floating fish farm structure has been analysed using REEF3D. The case was studied with an application of a mooring system on the floating aquaculture structure. Mooring system used in this case was an imitation of already existing mooring systems used for TLP (Tension Leg Platform) and FPSO (Floating Production Storage and Offloading) platforms. CFD model is new generation tool in design and engineering challenges. This preliminary study of the structures motion provides the basis for further research on the mooring configurations.</p> |
|---|

Keywords:

| |
|--------------------------------|
| 1. Moored-Floating Structures |
| 2. CFD |
| 3. Fluid-Structure Interaction |
| 4. REEF3D |

Acknowledgments

I would like to thank my supervisors who were an example of inspiration and who encouraged me during the whole period of my work on my Master's thesis.

Contents

| | | |
|----------|--|-----------|
| 1 | Introduction | 1 |
| 1.1 | Objectives of the Study | 2 |
| 2 | Numerical Model | 3 |
| 2.1 | Governing Equations | 3 |
| 2.2 | Numerical Treatment of Governing Equations | 4 |
| 2.3 | Convection Discretization | 4 |
| 2.4 | Discretization in Time | 5 |
| 2.4.1 | Adaptive Time Stepping | 5 |
| 2.5 | Turbulence Model | 6 |
| 2.6 | Pressure | 6 |
| 2.7 | Numerical Grid | 7 |
| 2.8 | Numerical Wave Tank | 7 |
| 2.8.1 | Boundary Conditions | 7 |
| 2.9 | Modelling the Free Surface | 8 |
| 2.9.1 | Level Set Method | 8 |
| 2.9.2 | Reinitialization | 8 |
| 2.9.3 | Wave Generation and Absorption | 9 |
| 2.10 | Wave Theory | 9 |
| 2.10.1 | Second Order Stokes Wave Theory | 9 |
| 2.11 | 6DOF Algorithm | 11 |
| 2.12 | Mooring Model | 14 |
| 3 | Results | 16 |
| 3.1 | Free Heave Decay Test | 16 |
| 3.1.1 | Mooring for Heave Decay Test | 17 |
| 3.2 | Floating Barge | 19 |
| 3.2.1 | Mooring for Floating Barge | 22 |
| 3.3 | 3D Simulation of Moored Fish Farm in Waves | 24 |
| 4 | Conclusions | 35 |

List of Figures

| | | |
|------|---|----|
| 2.1 | 6 Degrees of Freedom [12] - Graphical representation | 11 |
| 2.2 | Discrete Cable: Mass Points (black points), Bars (vectors) [15] | 14 |
| 2.3 | Geometrical Constraint [15] | 15 |
| 3.1 | The Contour Represents the Water Surface Motion | 17 |
| 3.2 | Convergence study of free heave decay of a circular cylinder. x axis: time. y axis: heave. | 18 |
| 3.3 | Effect of change of cylinder diameter on heave. | 19 |
| 3.4 | Effect of change of mooring line weight on the heave motion of the cylinder. | 20 |
| 3.5 | Effect of change of mooring line stiffness on the heave motion of the cylinder (weight 0.001 kg/m). | 21 |
| 3.6 | Effect of change of mooring line stiffness on the heave motion of the cylinder (weight 0.1 kg/m). | 22 |
| 3.7 | Numerical Wave Tank Schematic Representation | 22 |
| 3.8 | Floating Barge | 23 |
| 3.9 | Floating Barge Wave Elevation with $H = 0.1 \text{ m}$ | 23 |
| 3.10 | Floating Barge Sway Results with $H = 0.1 \text{ m}$ | 24 |
| 3.11 | Floating Barge Heave Results with $H = 0.1 \text{ m}$ | 25 |
| 3.12 | Floating Barge Pitch Results with $H = 0.1 \text{ m}$ | 26 |
| 3.13 | $t/T = 6.3$ with $H = 0.1 \text{ m}$ | 27 |
| 3.14 | Floating Barge Wave Elevation with $H = 0.04 \text{ m}$ | 27 |
| 3.15 | Floating Barge Sway Results with $H = 0.04 \text{ m}$ | 28 |
| 3.16 | Floating Barge Heave Results with $H = 0.04 \text{ m}$ | 28 |
| 3.17 | Floating Barge Pitch Results with $H = 0.04 \text{ m}$ | 29 |
| 3.18 | Mooring Applied Sway Results with $H = 0.1 \text{ m}$ | 29 |
| 3.19 | Mooring Applied Heave Results with $H = 0.1 \text{ m}$ | 30 |
| 3.20 | Mooring Applied Pitch Results with $H = 0.1 \text{ m}$ | 30 |
| 3.21 | Initial State | 31 |
| 3.22 | Under Action of Wave Forces | 31 |
| 3.23 | Strained Mooring Lines Design | 32 |

| | |
|--|----|
| 3.24 3D Floating Structure | 32 |
| 3.25 Three-dimensional structure motion with horizontal velocity x | 33 |
| 3.26 Sway Motion of 3D Floating Structure | 33 |
| 3.27 Heave Motion of 3D Floating Structure | 33 |
| 3.28 Pitch Motion of 3D Floating Structure | 34 |

Chapter 1

Introduction

Fluid-structure interaction has an essential role in any kind of offshore activities. The numerical model is implemented in the open-source CFD code REEF3D. To resolve engineering problems we need to know the nature of the complex fluid surface behaviour which includes phenomena as wave-breaking [4, 2], currents and turbulence models for the solution of which we resort Navier-Stokes equation. To perform numerical modelling with taking into consideration all above-mentioned aspects REEF3D software was used which allows not only to calculate the complex behaviour fluid surface and structure on it but also design a mooring system [15]. In addition to this, the model has been used extensively for complex wave hydrodynamics problems in the field of coastal and ocean engineering such as wave energy converter devices [13], non-breaking wave forces [14], and breaking wave forces [5]. Another significant issue related to coastal engineering is the coastal area erosion due to breaking waves [1]. The engineering design becomes more complicated when it comes to floating structures [6] in the deep-water environment. There are numerous floating structures such as floating oil platforms, floating barges. The thesis was prepared on the basis of numerical modelling of the fluid-structure interaction with an application of numerical wave models using [16] REEF3D software. This software allows creating numerical wave tank [11] in which experiments are carried out.

Mooring analysis includes loads in mooring systems on fish farms, feed barges or other floating structures. The goal is to model cost efficient mooring configuration, while still providing safe solutions, reducing the risk of contamination and fish escape. This means that mooring system should be analysed with use of calculation software. Floating bodies are often sensitive to wave loads and using REEF3D configurations we can perform an analysis of both, regular and irregular sea states. In this master thesis task, it was only considered regular sea states. Marine operations of various equipment require knowledge of the weather windows where the structure can withstand the loads caused by winds, waves, and currents. Based on our analysis we can visualize the load distributions in the components as well as fluid-structure

interaction. Stiffness and the design of mooring system are also essential to get a correct response of installation. Because of this, couple analysis with a different kind of mooring system will be performed for receiving the most accurate results. Stability of the structure is taken into account based on different levels of submergence of the moored floating body. Key parameters for this condition are the centre of gravity, buoyancy, metacentric height and righting moment.

1.1 Objectives of the Study

Floating bodies and moorings for them are modelled in the REEF3D. By entering wave data, the software calculates the 6DOF motion the floating body is subjected to. This facilitates optimization of components of which the mooring system consists. The Master thesis task involves numerical modelling of floating bodies on waves. This includes both freely floating bodies and moored bodies. The numerical model is built according to experimental data characteristics. Based on this model, performed simulations on REEF3D are compared with experimental data results, extracted from scientific sources. The influence of the incident wave characteristics and the effect of the aspect ratio of the structure on the motion of a freely floating structure was studied. After the comparison of results for freely floating structures, the algorithm was applied for mooring of floating body in waves.

Chapter 2

Numerical Model

This chapter deals with the basic concepts of CFD method which is employed in REEF3D software. The purpose is to give theoretical highlights of working principle of the software.

2.1 Governing Equations

The behaviour of viscous and incompressible fluids are described with Navier-Stokes equations [9] which are based upon the momentum conservation principle. On the right-hand side of the equations, there are the viscous and the pressure terms which are representative of the surface forces and gravity which is volume force whereas the transient and the convective terms are on the left-hand side of the equations.

$$\frac{\partial u_i}{\partial x_i} = 0 \quad (2.1)$$

$$\frac{\partial u_i}{\partial t} + u_j \frac{\partial u_i}{\partial x_j} = -\frac{1}{\rho} \frac{\partial p}{\partial x_i} + \frac{\partial}{\partial x_j} \left[\nu \left(\frac{\partial u_i}{\partial x_j} + \frac{\partial u_j}{\partial x_i} \right) - \overline{u'_i u'_j} \right] + g_i \quad (2.2)$$

In the formula u is velocity over time t , ρ is fluid density, p is pressure, ν is the kinematic viscosity, g is gravity acceleration and $\overline{u'_i u'_j}$ is representing Reynolds stresses. This nonlinear Reynolds stress term requires additional modeling to close the RANS equation which leads to creation of turbulence models in Chapter 2.5.

2.2 Numerical Treatment of Governing Equations

To numerically determine the fluid flow, by the application of numerical methods, the governing equations have to be discretized. There are different methods of discretization in CFD model. The one applied in REEF3D software is Finite Difference Method (FDM). In this method, a starting point is a differential form of conservation equation. Grid covers the whole domain where partial derivatives are replaced by approximated differential equations. Approximations are done in terms of nodal values of the functions where the results are represented in one algebraic equation per grid node. The variable value of that and neighbour nodes appear as unknowns. FDM is applicable to structured grids where the grid lines serve as local coordinate lines. To obtain the approximations to first and second derivatives of the variables with respect to the coordinates the Taylor series expansion is used. This method is also used for the interpolation purposes to obtain variable values out of grid points. FDM is beneficial due to the simplicity of application and efficiency on the structured grid. In addition, it enables high order schemes on regular grids. A possible disadvantage of FDM can be the restriction to simple geometries in complex flows, however, it can be overcome in a special way. The following concepts explain the operation of computational fluid dynamics model:

- **Accuracy:** This concept defines the level of precision related to truncation error which is the difference between an exact solution and numerical approximation. After discretization which in this case based on Taylor series expansion if the difference between an exact solution and numerical approximation tends to zero then truncation error also approaches zero which leads to higher level of accuracy.
- **Stability:** Stability of a numerical scheme refers to its ability to converge to the exact solution. A scheme is said to be stable when there happens to be an upper and lower bound on the errors. Otherwise, with unbound errors, the solution will “blow up” and the numerical approximation will be nowhere close to the exact solution.

2.3 Convection Discretization

There are numerous ways for discretization in FDM. Weighted Essentially Non-Oscillatory (WENO) schemes can handle large gradients very accurately by taking local smoothness into account. It is balanced by the implementation of fifth-order WENO in the conservative finite difference framework for the convection discretization of the flow velocities. These stencils are weighted depending on their smoothness,

with the smoothest stencil contributing the most significantly.

$$u_i \frac{\partial u_i}{\partial x_i} \approx \frac{1}{\Delta x} (\tilde{u}_{i+1/2} u_{i+1/2} - \tilde{u}_{i-1/2} u_{i-1/2}) \quad (2.3)$$

The convection velocity \tilde{u} is obtained at the cell phases through interpolation.

2.4 Discretization in Time

For discretization in time high numerical accuracy and stability is required as it also has transient nature in CFD model. The explicit third-order TVD Runge-Kutta scheme was used which is applicable for velocities and scalar values.

$$\begin{aligned} \phi^{(1)} &= \phi^n + \Delta t L(\phi^n) \\ \phi^{(2)} &= \frac{3}{4}\phi^n + \frac{1}{4}\phi^{(1)} + \frac{1}{4}\Delta t L(\phi^{(1)}) \\ \phi^{n+1} &= \frac{1}{3}\phi^n + \frac{2}{3}\phi^{(2)} + \frac{2}{3}\Delta t L(\phi^{(2)}) \end{aligned} \quad (2.4)$$

The term ‘L’ represents the spatial discretization and ϕ is random variable.

2.4.1 Adaptive Time Stepping

For the maintenance of simulation stability, the fluid should progress at the speed of one cell per time-step. This condition is called Courant-Friedrichs-Lewy (CFL) which has the following form in one-dimensional representation.

$$C = \frac{u\Delta t}{\Delta x} \leq C_{max} \quad (2.5)$$

where C is the Courant number which is dimensionless unit, u is magnitude of velocity δt is time step and δx is the length interval, $C_{max} = 1$ CFL number inside the limit is controlled by adaptive time stepping. Time-step size δt is defined in the following way:

$$\Delta t \leq 2 \left(\left(\frac{|u|_{max}}{dx} + D \right) + \sqrt{\left(\frac{|u|_{max}}{dx} + D \right)^2 + \frac{4|S_{max}|}{dx}} \right)^{-1} \quad (2.6)$$

with

$$D = \max(\nu + \nu_t) \cdot \left(\frac{2}{(dx)^2} + \frac{2}{(dy)^2} + \frac{2}{(dz)^2} \right) \quad (2.7)$$

Where u is velocity, D diffusion and S is source term.

2.5 Turbulence Model

For the current master thesis $k - w$ turbulence model [10, 18] was used. This two-equation turbulence model is used as a closure for RANS equations. This system operates on the basis of prediction of turbulence using two partial differential equations for two variables, k and w . Where k variable is turbulence kinetic energy and w is a specific rate of dissipation. The standard form for $k - w$ turbulence model is:

$$\frac{\partial k}{\partial t} + u_j \frac{\partial k}{\partial x_j} = \frac{\partial}{\partial x_j} \left[\left(\nu + \frac{\nu_t}{\sigma_k} \right) \frac{\partial k}{\partial x_j} \right] + P_k - \beta_k k \omega \quad (2.8)$$

$$\frac{\partial \omega}{\partial t} + u_j \frac{\partial \omega}{\partial x_j} = \frac{\partial}{\partial x_j} \left[\left(\nu + \frac{\nu_t}{\sigma_\omega} \right) \frac{\partial \omega}{\partial x_j} \right] + \frac{\omega}{k} \alpha P_k - \beta \omega^2 \quad (2.9)$$

The P_k is turbulent production rate. Coefficients $\alpha = 5/9$, $\beta_k = 9/100$, $\beta = 3/40$, $\sigma = 2$, $\sigma_\omega = 2$

2.6 Pressure

In comparison to other variables of Navier-Stokes equation, there is no obvious equation from which solution for pressure can be derived. Chorins's projection method can be used where the solution for the velocity depends on previous time steps. In this case for an intermediate velocity u_i^* momentum equation can be used without pressure gradient:

$$\frac{\partial u_i^*}{\partial t} + u_j^n \frac{\partial u_i^n}{\partial x_j} = \frac{\partial}{\partial x_j} \left[(\nu + \nu_t) \left(\frac{\partial u_i^n}{\partial x_j} + \frac{\partial u_j^n}{\partial x_i} \right) \right] + g_i \quad (2.10)$$

Here intermediate velocity u_i^* is not divergence free, or:

$$\frac{\partial u_i^*}{\partial x_i} \neq 0 \quad (2.11)$$

To create divergence-free flow field the pressure should be included into the continuity equation:

$$\frac{\partial}{\partial x_i} \left(\frac{1}{\rho(\phi^n)} \frac{\partial p^{n+1}}{\partial x_i} \right) = \frac{1}{\Delta t} \frac{\partial u_i^*}{\partial x_i} \quad (2.12)$$

This is a Poisson equation which is a system of linear equations, solved by appropriate linear solvers. REEF3D uses the HYPRE library for that. Due to the difference in density between phases the matrix coefficients are anisotropic. Therefore the com-

putational cost is very demanding. When the pressure for the new time step p^{n+1} is defined, it can be used to correct the intermediate velocity field u_i^* , making it divergence free:

$$u_i^{n+1} = u_i^* - \frac{\Delta t}{\rho(\phi^n)} \frac{\partial p^{n+1}}{\partial x_i} \quad (2.13)$$

2.7 Numerical Grid

In the REEF3D CFD model, the Cartesian grid had been used for the generation of the mesh. This type of grid allows to easily identify the neighbouring points around the point and assess them efficiently which consequently affect on the calculation speed of CFD codes.

2.8 Numerical Wave Tank

Numerical wave tank is the numerical volume where simulations with waves and floating structures are taking place. Numerical wave tank design is fast, easy and most of all is cost efficient in implementation, and arrangement in comparison with laboratory simulations. The numerical tank is covered with a grid of specific mesh size based on the requirements of the simulations performed. For higher precision, the finer mesh size is used however for less accuracy demanding simulations coarser grid size is introduced. NWT is divided into three zones: wave generation, wave tank and numerical beach. This configuration is specific for the given task, however, it can differ in other tasks. Wave generation zone is one wavelength long and numerical beach zone is two wavelengths long.

2.8.1 Boundary Conditions

There are several boundary conditions in REEF3D's NWT: wave generation, inflow, outflow, numerical or active beach. The ones we are interested in for current task are solid boundary and wave generation and absorption. Solid boundaries can be defined as slip or non-slip. In this thesis task, it was considered as non-slip boundary condition which means that velocity of a fluid particle near the wall is equal to zero with respect to it. Together with the non-slip condition the wall roughness also should be included in the calculation which is done using Schlichtings formula:

$$u^+ = \frac{1}{\kappa} \ln \left(\frac{30y}{k_s} \right) \quad (2.14)$$

here u^+ is dimensionless wall velocity, $k = 0.4$ is the von Karman constant obtained from experiments, y water depth, k_s equivalent sand roughness. Turbulent production is equal to the dissipation k near the wall in REEF3D NWT. For the specific turbulent dissipation ω the wall function for the bed cell with distance δy_p from the wall to the cell center is:

$$\epsilon_{wall} = -\frac{c_\mu^{3/4} k_w^{1/2} U_w^+}{\Delta y_p} \quad (2.15)$$

From this formula, we can obtain the turbulent dissipation ϵ . We put ϵ value into the equation 2.8 and after the integration, we get the following formula:

$$\int (P_k - \epsilon_{wall}) \rho = \left[\frac{\tau_w u_w}{\Delta y_p} - \frac{c_\mu^{3/4} k_w^{1/2} U_w^+}{\Delta y_p} \right] \quad (2.16)$$

2.9 Modelling the Free Surface

2.9.1 Level Set Method

In REEF3D the flow is modelled as a two-phase system. The interface between the fluids interfaces is defined as zero-contour of level set functions. Moving away from the interface, the level set function is defined as a distance function.

$$\phi(\vec{x}, t) \begin{cases} > 0 & \text{if } \vec{x} \text{ is in phase 1} \\ = 0 & \text{if } \vec{x} \text{ is at the interface} \\ < 0 & \text{if } \vec{x} \text{ is in phase 2} \end{cases} \quad (2.17)$$

The movement of the interface is characterized by the convection of the level set function determined by

$$\frac{\partial \phi}{\partial t} + u_j \frac{\partial \phi}{\partial x_j} = 0 \quad (2.18)$$

2.9.2 Reinitialization

This study uses a PDE based reinitialization procedure presented by.

$$\frac{\partial \phi}{\partial \tau} + S(\phi) \left(\left| \frac{\partial \phi}{\partial x_j} \right| - 1 \right) = 0 \quad (2.19)$$

where $S(\phi)$ is the smooth signed function by

$$S(\phi) = \frac{\phi}{\sqrt{\phi^2 + \left| \frac{\partial \phi}{\partial x_j} \right|^2 (\Delta x)^2}} \quad (2.20)$$

where $S(\phi)$ is the smooth signed function at the cell surface the level set function is obtained by:

$$\phi_{i+1/2} = \frac{1}{2} (\phi_i + \phi_{i+1}) \quad (2.21)$$

2.9.3 Wave Generation and Absorption

In REEF3D wave generation and absorption is performed by relaxation method (RM) and active wave absorption method (AWA).

Relaxation Method

In the relaxation method, the relaxation function is used for the introduction of the velocity, pressure and free surface values into the NWT for wave generation purposes. Velocities are smoothly reduced to zero, the free surface is brought to still water level, the pressure is relaxed to hydrostatic value for still water level to effectively absorb the incident waves at the numerical beach and prevent unwanted reflections. It is carried out in the following way in the dominating relaxation zones.

$$F(\tilde{x})_{relaxed} = \Gamma(\tilde{x})F_{analytical} + (1 - \Gamma(\tilde{x}))F_{computational} \quad (2.22)$$

Where \tilde{x} is normalized length of relaxation zone and $\Gamma_R(\chi_R)$ is relaxation function. The equation shown below is another form of relaxation function proposed by Jacobsen.

$$\Gamma_R(\chi_R) = 1 - \frac{\exp(\chi_R^{3.5}) - 1}{\exp(1) - 1} \text{ for } \chi_R \in [0; 1] \quad (2.23)$$

The function $\Gamma_R(\chi_R)$ varies depending on the location of the relaxation zone. In the case of numerical beach zone, the formula will represent the transformation from computational values to analytic.

2.10 Wave Theory

2.10.1 Second Order Stokes Wave Theory

The second order Stokes theory developed by Stokes in 1847, is applicable when the ratio H/d is small. So, the theory is applicable in deep waters and some range of intermediate waters. It formulates the wave characteristics in form of a power series

of the wave steepness H/L . The non-dimensional factor used in the power series known as the perturbation factor. Here, η , Φ , u and w are:

$$\eta = a \cos(kx - \omega t) + \frac{\pi H}{8} \frac{H}{L} \frac{\cosh kd(2 + \cosh 2kd)}{\sinh^3 kd} \cos 2(kx - \omega t) \quad (2.24)$$

where a is wave amplitude, $\omega = 2\pi/T$ is the observed wave angular frequency, $k = 2\pi/\lambda$ is wave number with wavelength, d is water depth, t is time and x the direction of propagation.

$$\Phi = \frac{ag}{\omega} \frac{\cosh k(d+z)}{\cosh kd} \sin(kx - \omega t) + \frac{3\pi CH}{16} \frac{H}{L} \frac{\cosh 2k(d+z)}{\sinh^4 kd} \sin 2(kx - \omega t) \quad (2.25)$$

$$u = \frac{\partial \Phi}{\partial x} = \omega a \frac{\cosh k(z+d)}{\sinh kd} \sin(kx - \omega t) + \frac{H}{L} \frac{3\pi^2 H}{4T} \frac{\cosh(2k(d+z))}{\sinh^4(kd)} \cos 2(kx - \omega t) \quad (2.26)$$

$$w = \frac{\partial \Phi}{\partial x} = \omega a \frac{\cosh k(z+d)}{\sinh kd} \sin(kx - \omega t) + \frac{H}{L} \frac{3\pi^2 H}{4T} \frac{\sinh(2k(d+z))}{\sinh^4(kd)} \sin 2(kx - \omega t) \quad (2.27)$$

2.11 6DOF Algorithm

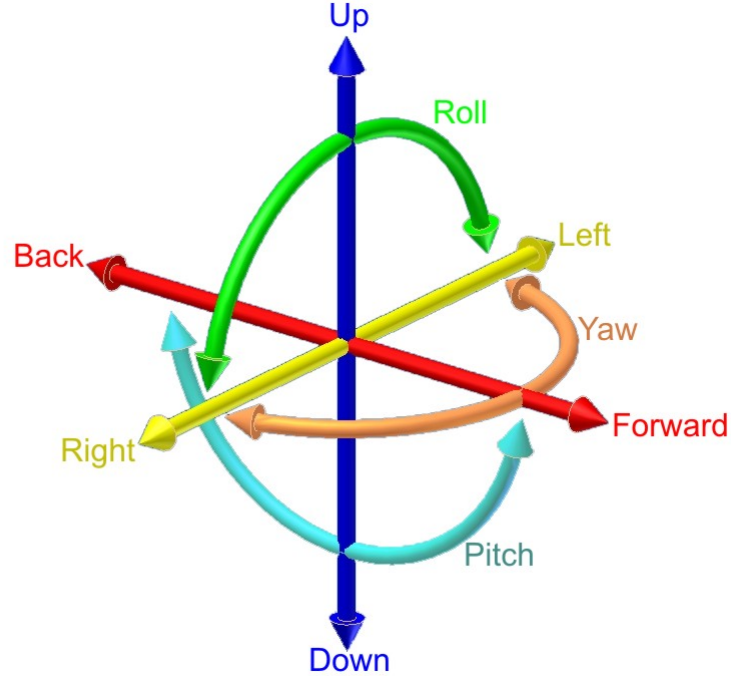


Figure 2.1: 6 Degrees of Freedom [12] - Graphical representation

To calculate the fluid-structure interaction the geometry of the solid body should be defined which is represented in the simple triangular surface mesh neglecting connectivity. The solid body is designed in ".stl" format which is available in CAD software. The ray-tracing algorithm is used for the connection of the surface mesh with the underlying Cartesian grid. Hereafter standard re-initialization algorithm is used to obtain distance properties in the vicinity of the solid body. The ray-tracing algorithm calculates the distances in an exact manner close to the solid boundary. The forces acting on the surface of the floating body can be determined for each coordinate direction separately using p and viscous stress tensor τ in this way:

$$F_{i,e} = \int_{\Omega} (-\mathbf{n}_i p + \mathbf{n}_i \cdot \boldsymbol{\tau}) d\Omega \quad (2.28)$$

The distance of the center of gravity from the origin of the body grid can be determined with:

$$\mathbf{r}_{cg} = \frac{1}{m} \int_V \mathbf{r} \rho_a dV \quad (2.29)$$

where r is the distance from each surface cell to the origin of the body-fitted coordinate system. Assuming that the origin of the body-fitted coordinate system is at the centre

of gravity of the floating body, r is the distance of each surface cell to the centre of gravity. Proceeding from this the moments can be calculated in the following way:

$$L_{i,e} = \int_{\Omega} \mathbf{r} \times (\mathbf{n}_i p + \mathbf{n}_i \cdot \boldsymbol{\tau}) d\Omega \quad (2.30)$$

The calculation of the discrete surface area in each grid cell can be accomplished with the help of a Dirac delta function:

$$d\Omega = \int \delta(\phi) |\nabla \phi| dx \quad (2.31)$$

The level set description advantage for the surface area is that intersections of the surface mesh with the underlying grid do not require explicit calculation. The free-floating algorithm has 6 Degrees of Freedom (6DOF) translation of which consists of three linear velocities u , v , ω and rotation has three angular velocities p , q and r . The location and orientation of the floating body is given by the position vector and the Euler angles.

$$\eta = (\eta_1, \eta_2) = (x_{cg}, y_{cg}, z_{cg}, \phi, \theta, \psi) \quad (2.32)$$

Calculation of moments of inertia for the 6DOF for the floating body by the introduction of two separate coordinate systems. The fluid flow, consequently the forces acting on the floating body and moments can be calculated in the inertial coordinate system. When the origin of non-inertial coordinate system coincides with the center of gravity, the moments of inertia are calculated only with main diagonal of the moment of inertia tensor:

$$\mathbf{I} = \begin{bmatrix} I_x & 0 & 0 \\ 0 & I_y & 0 \\ 0 & 0 & I_z \end{bmatrix} = \begin{bmatrix} mr_x^2 & 0 & 0 \\ 0 & mr_y^2 & 0 \\ 0 & 0 & mr_z^2 \end{bmatrix} \quad (2.33)$$

where r_x , r_y , r_z are the distances from the centre of gravity along the x , y and z directions. From the inertial frame, the forces and moments can be expressed in the non-inertial coordinate system with rotation matrix J^{-1}_1 which consists of three rotations around the axis of the coordinate system:

$$a_{fb} = \begin{bmatrix} c\psi c\theta & s\psi c\theta & -s\theta \\ -s\psi c\phi + s\phi s\theta c\psi & c\psi c\phi + s\phi s\theta s\psi & s\phi c\theta \\ s\theta s\psi + c\phi s\theta c\psi & -s\phi c\psi + c\phi s\theta s\psi & c\theta s\phi \end{bmatrix} \mathbf{a}_e = \mathbf{J}_1^{-1} \mathbf{a}_e \quad (2.34)$$

Here \sin denoted as s and \cos is denoted as c , a_{fb} is a vector on the reference frame of the floating body and a_e is inertial coordinate system vector. From the calculation of forces, momentum and moments of inertia we can obtain dynamics of the rigid

body.

$$\begin{aligned} F_i &= \mathbf{J}_1^{-1} F_{i,e} = [X, Y, Z] \\ L_i &= \mathbf{J}_1^{-1} L_{i,e} = [K, M, N] \end{aligned} \quad (2.35)$$

here

$$\begin{aligned} [m(\dot{u} - vr + wq)] &= X \\ [m(\dot{v} - wp + ur)] &= Y \\ [m(\dot{w} - uq + vp)] &= Z \\ [I_x \dot{p} + (I_z - I_y) qr] &= K \\ [I_y \dot{q} + (I_x - I_z) rp] &= M \\ [I_z \dot{r} + (I_y - I_x) pq] &= N \end{aligned} \quad (2.36)$$

Here, u, v, w, p, q and r are linear and angular velocity values obtained from previous case and $\dot{p}, \dot{q}, \dot{r}$ are acceleration values coming from an explicit calculation. Linear and angular velocities $\dot{\phi}$ can be obtained from second-order Adams-Bashforth scheme from the old time step. We can also use this formula for calculation of position and orientation vector ϕ of floating rigid structure.

$$\begin{aligned} \dot{\phi}^{n+1} &= \dot{\phi}^n + \frac{\Delta t}{2} (3\ddot{\phi}^{n+1} - \ddot{\phi}^n) \\ \phi^{n+1} &= \phi^n + \frac{\Delta t}{2} (3\dot{\phi}^{n+1} - \dot{\phi}^n) \end{aligned} \quad (2.37)$$

Proceeding from this we can observe that the floating body dynamics can be solved in an explicit way. In the reference frame of the floating body, the dynamic rigid body equations have been solved where translations and orientations of the rigid body were also calculated. Rotation matrix J_2 [17] is used to transform the angular velocities where s, c and t stands for \sin, \cos and \tan consequentially.

$$\dot{\eta}_2 = \begin{bmatrix} 1 & s\phi t\theta & c\phi t\theta \\ 0 & c\phi & -s\phi \\ 0 & s\phi/c\theta & c\phi/c\theta \end{bmatrix} v_2 = \mathbf{J}_2 v_2 \quad (2.38)$$

The boundary condition for the velocities on the solid-fluid interface result from the motion of the solid body with respect to its center of gravity.

$$u_i = \dot{\eta}_1 + \dot{\eta}_2 \times \mathbf{r} \quad (2.39)$$

There is a possibility of occurrence of pressure oscillations near the solid structure.

This is because solid cells are turning to fluid cells or vice versa. In order to avoid this phenomenon the field extension method needs to be applied which is an adaptation to the ghost cell immerse boundary method. A zero gradient boundary condition is used for the pressure to avoid this phenomenon for non-moving boundaries. Near the floating body to maintain a physical pressure gradient, following boundary condition for pressure is used:

$$\frac{\partial p}{\partial x_i} = -\frac{1}{\rho} \frac{Du_i}{Dt} \quad (2.40)$$

One of the possibilities to find u_i is an evaluation of the momentum equation. In this case, we differentiate equation 2.39 with respect to time and taking pressure values for ghost cell.

$$\frac{Du_i}{Dt} = \frac{\partial}{\partial t} (\dot{\eta}_1 + \dot{\eta}_2 \times \mathbf{r}) \quad (2.41)$$

Due to the motion of the floating rigid body when the cells of rigid body turn to the fluid cell we use velocities from equation 2.39 to calculate pressure through the interpolation from the fluid. The model was implemented in REEF3D successfully and presented in [7, 3].

2.12 Mooring Model

The used mooring model is based on a numerical approach presented in [15]. This model implies the use of mooring lines (ropes, chains) which has its own physical specifications. In addition, this numerical model of mooring system experiences all the loads and physical forces acting on it which are gravity forces \vec{F}_G and hydrodynamic force \vec{F}_H . For mooring system, the moment forces are not considered as it is a flexible system.

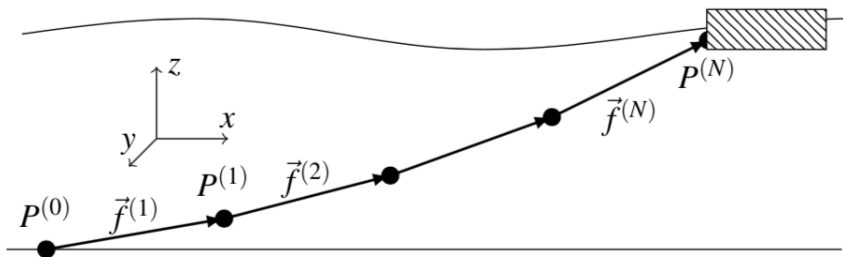


Figure 2.2: Discrete Cable: Mass Points (black points), Bars (vectors) [15]

$$\vec{F}_G^{(\nu)} = q\vec{g} \cdot \left(\frac{a^{(\nu)} + a^{(\nu+1)}}{2} \right), \quad \nu = 1, \dots, N-1 \quad (2.42)$$

here a is the length of the mooring elements, N mass points which are distributed all over the length, q the specific material weight per length in the fluid and \vec{g} a unit vector pointing in negative z direction. The below-shown formula represents the force equilibrium in the mooring system.

$$\vec{f}^{(\nu+1)} F_T^{(\nu+1)} - \vec{f}^{(\nu)} F_T^{(\nu)} = -\vec{F}_G^{(\nu)} \quad (2.43)$$

here \vec{f} represents inner tension forces, F_T is the magnitude of tension forces. For the solution of this problem the iterative method should be used, however, there is another lemma that should be solved, that is - the number of bars exceeds the number of inner knots. For this task solution the iterative method should be used, however, there is another problem that should be solved, that is - the number of bars exceeds the number of inner knots. Thus, the system is undetermined and has to be closed by adding a geometrical constraint. It accomplishes the coherence of the cable during the deformation in a physical way and is determined from the known distance between the two end points [15] (see figure 2.3).

$$\sum_{\nu=1}^{N+1} \vec{f}^{(\nu)} a^{(\nu)} = \vec{c} \quad (2.44)$$

where \vec{c} is vector (see figure 2.3)

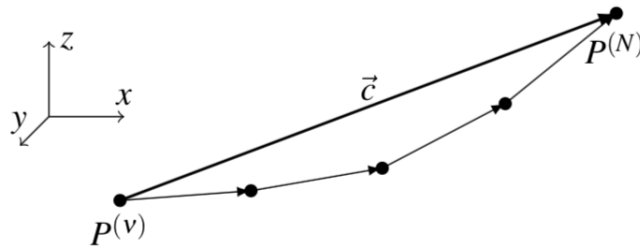


Figure 2.3: Geometrical Constraint [15]

Chapter 3

Results

3.1 Free Heave Decay Test

In this test represented free falling rigid body where we observe heave motion depending on its density, physical properties of air and water. The results have been compared with experimental data from scientific data [19]. Experimental results were taken from laboratory tests and compared with the numerical model. The test is performed in 2D representation in REEF3D software. Physical properties of circular cylinder are following: diameter $D = 0.1524 \text{ m}$, density $\rho = 500 \text{ kg/m}^3$. The cylinder is partially submerged and its centre is located at 0.0254 m above the water surface in the numerical tank from which it was released at time $t = 0 \text{ s}$. The density of water $\rho = 1000 \text{ kg/m}^3$, density of air $\rho = 1.2 \text{ /m}^3$, gravity acceleration $g = -9.81 \text{ m/s}^2$, water and air viscosities $\mu_{water} = 1.0 * 10^{-3} \text{ Pa/s}$, $\mu_{air} = 1.0 * 10^{-5} \text{ Pa/s}$ respectively. After the release we will observe oscillations of the rigid body and consequently generation of waves that will fade away very quickly. This phenomenon related to the gravity effect of the water.

The numerical tank where the simulations have been performed are following: length - 6 m height - 2 m . The CFD model was generated on the mesh size are following: $dx = 0.006$, $dx = 0.01$, $dx = 0.0125$ and $dx = 0.02 \text{ m}$. These mesh sized are chosen to obtain the highest accuracy from the numerical simulation in order to obtain the results with minimum deviation from experimental data. In this case, no turbulence model is included in numerical modelling.

In the figure below is shown the heave motion of the cylinder for each second of the simulation. We can observe the formation of waves that are generated from cylinder entrance to the liquid phase. They move symmetrically in both directions. At the third second of the simulation, the water surface around the cylinder is calm again.

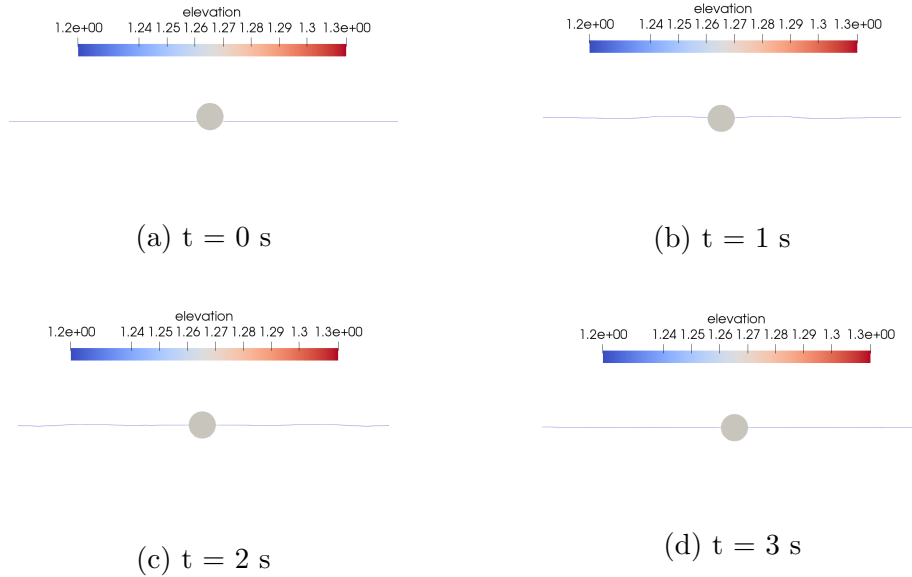


Figure 3.1: The Contour Represents the Water Surface Motion

The same representation can be found in the figure 3.2 below which is the graphical interpretation of cylinder motion.

As we can see from the figure 3.2 the results obtained from laboratory experiments match with numerical simulations obtained from REEF3D software. The smallest deviation between experimental and numerical data is obtained from mesh size $dx = 0.006$ m. In the 3.3 there are represented results of numerical simulations with different cylinder diameter but with constant density parameter. As we can observe from the plots, with an increase of cylinder diameter the frequency of oscillations decrease. In addition, we can observe from plots that the amplitude of heave motion increases with the increase of cylinder diameter. This is due to the fact that the area of buoyancy force applied to the cylinder increases which leads to an increase of amplitude in heave motion. The minimum mesh size chosen for this test is $dx = 0.01$ m.

3.1.1 Mooring for Heave Decay Test

This test has been performed for the free-falling cylinder from previous case 3.1 with the same physical parameters for the rigid body itself and phases in which the test is taking place. It should be noted that the simulation of floating structure with mooring lines hold in REEF3D software using CFD numerical model. The mesh size

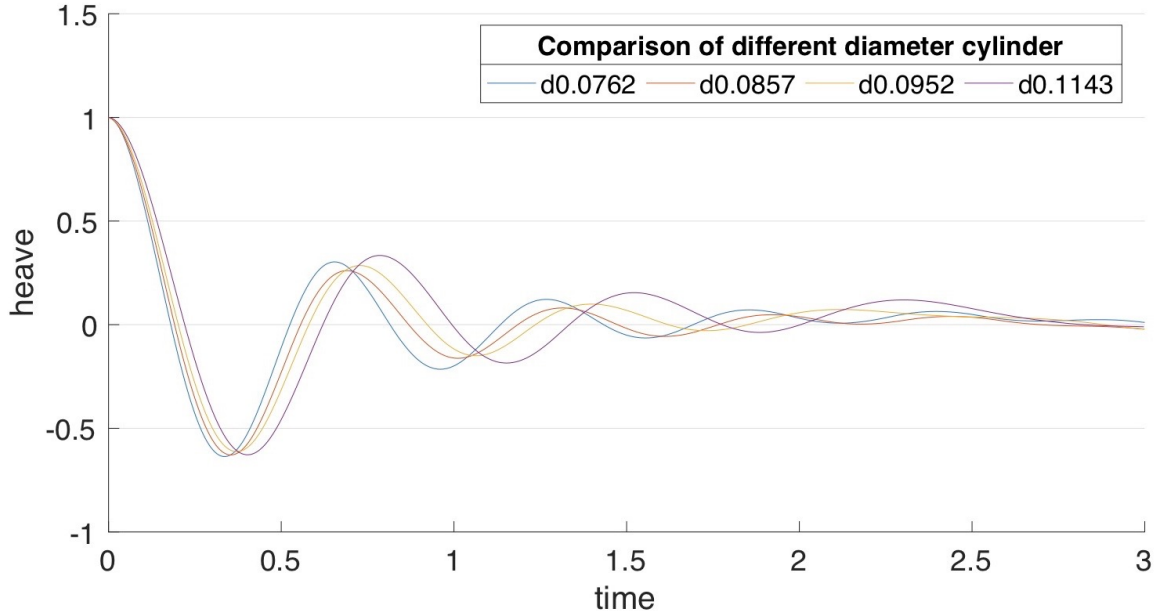


Figure 3.3: Effect of change of cylinder diameter on heave.

difference between the mooring lines effect on the heave motion behaviour of the cylinder is almost negligible. The stiffness parameters taken into consideration in this case are $1 \cdot 10^9 \text{ N/m}$ and 10 N/m . However, from the figure 3.6 we can observe that results are different from the previous ones. The stiffness parameters remained the same as in previous simulation 3.5 but different mooring line weight which is equal to 0.1 kg/m was chosen. The purpose of this simulation was to define the effect of weight and stiffness of mooring lines on the motion of the cylinder. Proceeding from obtained results we can conclude that the most important parameter in the design of numerical mooring lines are weight and depending on the value of weight the stiffness which can affect the cylinder motion. Based on this parameters we will be able to design and optimize numerical mooring lines for next cases.

3.2 Floating Barge

In this case, the numerical simulations were performed for the floating barge for the 2D case with 3DOF (x,y, z-direction surge, heave, and pitch) and compared with results from experimental data [8]. The simulations have been performed with mesh size $dx = 0.004$, $dx = 0.005$, $dx = 0.01$ and $dx = 0.015 \text{ m}$. Length of numerical wave tank is 20 m and height is 0.8 m . Dimensions of the floating barge are following: length 0.30 m , height 0.20 m with density of $\rho = 500 \text{ kg/m}^3$. The wave height acting on the floating body is $H = 0.1 \text{ m}$, period $T = 1.2$ seconds wavelength $\lambda = 1.936 \text{ m}$,

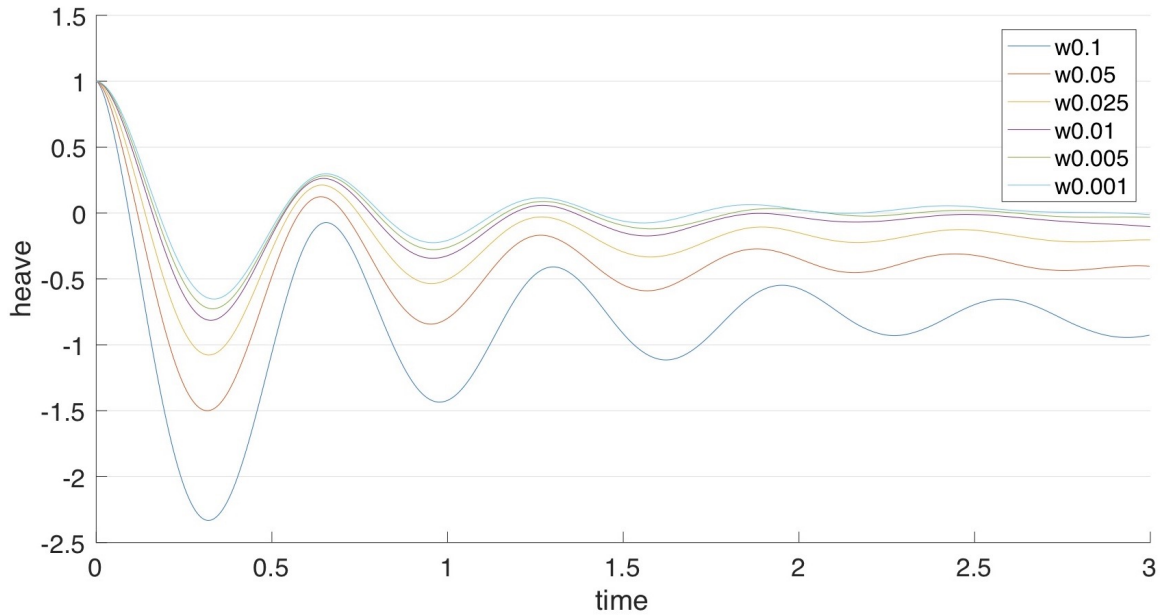


Figure 3.4: Effect of change of mooring line weight on the heave motion of the cylinder.

water depth 0.4 m . The numerical wave tank is subdivided into three parts: wave generation zone, wave tank, and numerical beach. This configuration is specific to the current task. For characterization of the waves, second-order Stokes wave theory was used. In the image 3.7 the scheme of the numerical wave tank was presented:

The total time for simulation is 14 s . In the plots below there are the graphical representation of results for the 3DOF motion of freely floating barge.

The figure 3.9 shows the comparison of the numerical model with experimental for the wave elevation. The convergence for wave elevation starts from $t/T = 6.3$. As we can observe from figure 3.9, the numerical data almost aligns with experimental data, however, there is a small difference among wave crests between $t/T = 6.3 - 9$ and small divergence in wave troughs from $t/T = 9 - 11.5$. The best approximation between numerical and experimental data is obtained with a mesh size $dx = 0.004\text{ m}$.

In the figure 3.10, results for surge have been presented where we can observe convergence between numerical and experimental data starts from $t/T = 6.3$. Starting from $t/T = 7.5$ there is an insignificant misalignment in frequency between numerical and experimental data. However, the results are perfectly matching in a frequency of waves. The finest mesh sizes which are matching experimental data are $dx = 0.004$ and $dx = 0.005\text{ m}$.

In the figure 3.11 we can observe a comparison of heave motion of the floating struc-

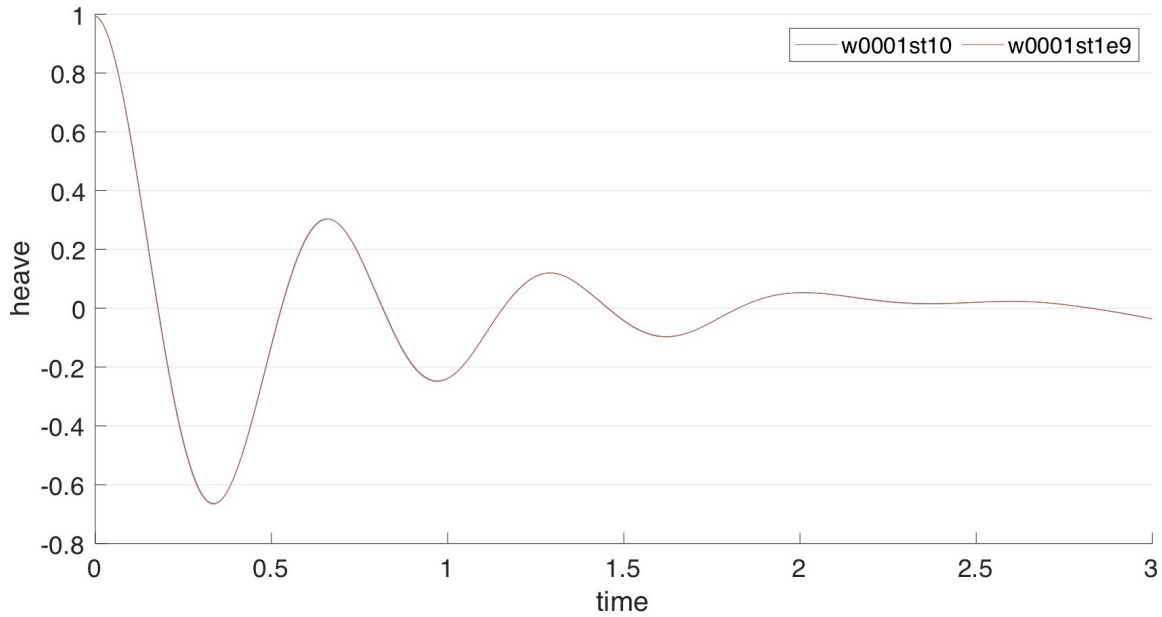


Figure 3.5: Effect of change of mooring line stiffness on the heave motion of the cylinder (weight 0.001 kg/m).

ture between experimental and numerical data. We can observe from the plot the convergence in wave crest form $t/T = 6.1 - 8$ of the between experimental and numerical data whereas the wave troughs are smaller in numerical one. After $t/T = 8$ we can observe an insignificant shift in frequency whilst the wave crests have the same height between numerical and experimental data.

In the figure 3.12 we can clearly observe the convergence between the numerical and experimental data from $t/T = 6.3 - 8$ after that time there is an insignificant misalignment in frequency starts as it was observed in the figure 3.11. In the image below we can observe the physical representation of the floating barge using Paraview software. In the image has been shown the floating barge on the free surface in the numerical wave tank at $t/T = 6$.

Another experiment was held with the same numerical tank configurations and floating barge. All the wave characteristics were the same. The only difference is the wave height which in this case is equal $H = 0.04 \text{ m}$. Also for this case, we have had experimental data [8] taken from laboratory tests which are used for comparison with numerical data obtained from the CFD model on REEF3D software. The results shown below are representing the same 3DOF motion of the floating barge. The numerical simulation results in case of $H = 0.04 \text{ m}$ have the same output as in case of $H = 0.1 \text{ m}$. For example: As we can observe from the 3.16 the wave crests are higher

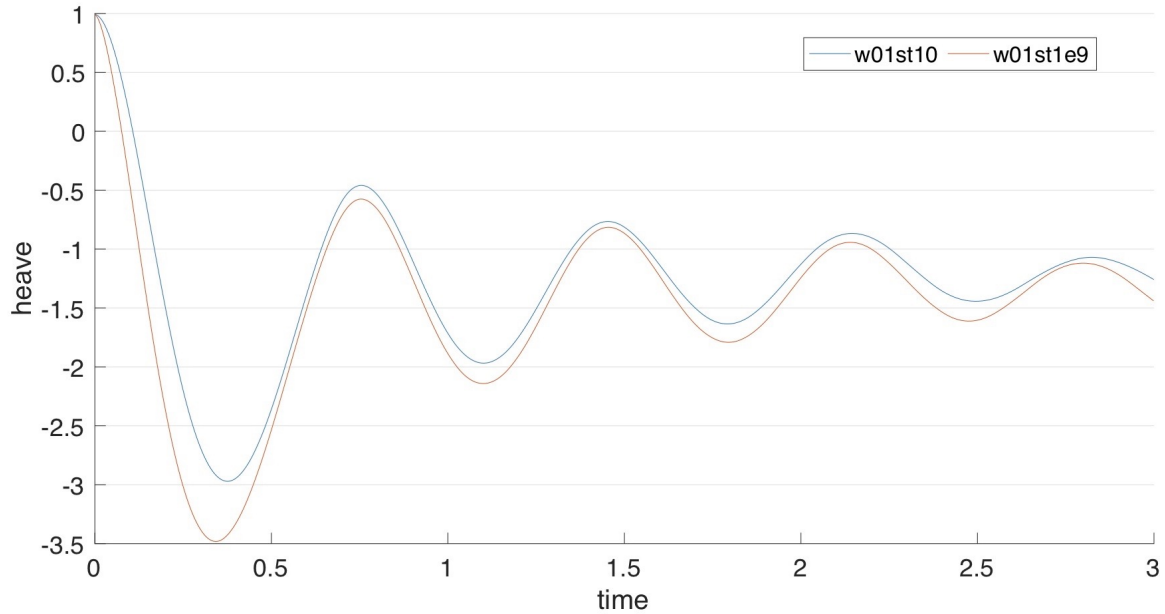


Figure 3.6: Effect of change of mooring line stiffness on the heave motion of the cylinder (weight 0.1 kg/m).

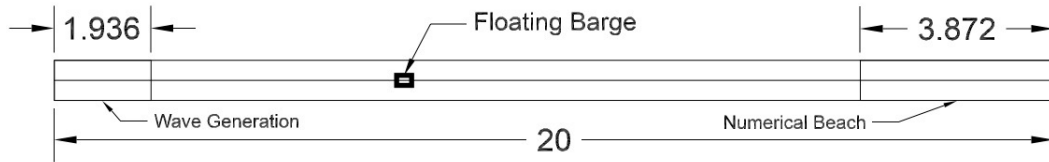


Figure 3.7: Numerical Wave Tank Schematic Representation

with respect to the experimental data at the beginning of the simulation, however, starting from 8 seconds of simulation the wave crests are matching each other. The wave troughs are shorter in the numerical results representation for wave elevation.

3.2.1 Mooring for Floating Barge

As in the case of heave decay test also for this numerical simulation, we do not have experimental data for comparison mooring results. However, in this case, we can use results of simulation coming from heave decay test and apply them in this case. In the numerical design of the mooring lines, in this case, we will use the most optimal configurations for floating barge based on the previous experience i.e. weight of mooring lines $m = 0.001 \text{ kg/m}$ stiffness $k = 1 * 10^9 \text{ N/m}$.

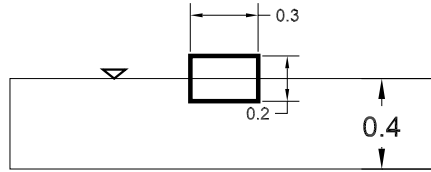
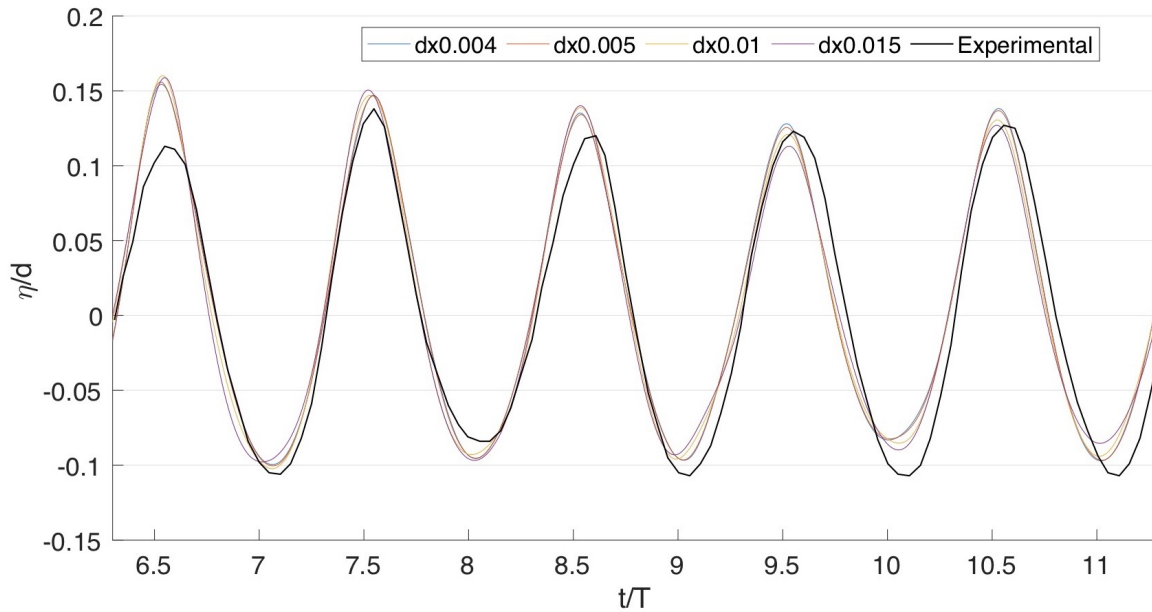
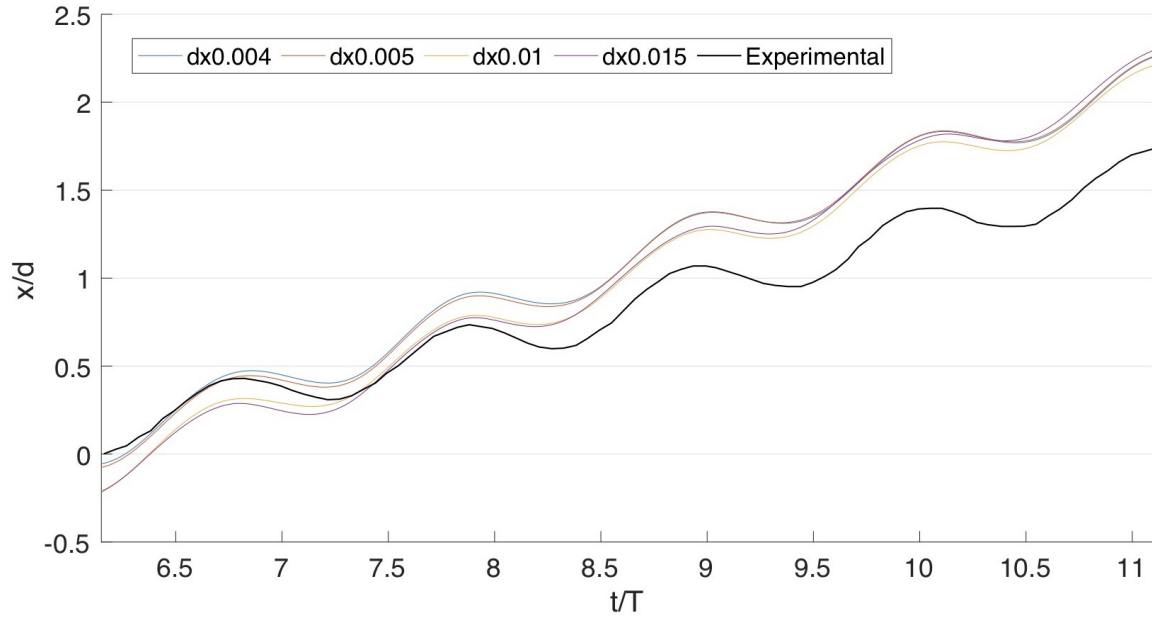


Figure 3.8: Floating Barge

Figure 3.9: Floating Barge Wave Elevation with $H = 0.1 \text{ m}$

The choice of these parameters is not random. The reason for this type of approach in design is to minimize the influence of mooring line on the 3DOF motion behaviour of the floating barge i.e. the mooring line is used only to keep the barge in place and not allow to have displacement from the original position under the action of waves. In the figures 3.18, 3.19, 3.20 are shown results for 3DOF of motion of mooring barge with numerically designed mooring lines where we can observe that they are not affected by the weight of the mooring lines. On the other side, we can see that on the heave and sway motion there are some sharp endings appearance on the wave crest starting from $t/T = 9$. These phenomena have not been observed in the previous experiments, therefore, we can assume that at the wave crest sudden pulling down of floating barge occur due to the mooring line.

Figure 3.10: Floating Barge Sway Results with $H = 0.1 \text{ m}$

3.3 3D Simulation of Moored Fish Farm in Waves

The three-dimensional simulation for floating aquaculture cage without nets with mooring was modelled on the basis of results of previous experiments of floating barges and mooring analysis on them. The structure was built in CAD software, imported in REEF3D simulation as a .stl file. The structure parameters are based on design aspects OceanFarm1 the world's largest floating fish farm which is currently under operation. Stability of the structure is taken into account based on different levels of submergence of the moored floating body. Key parameters for this condition are centre of gravity, buoyancy, metacentric height and righting moment. In addition, turbulence parameters are also taken into consideration.

| | Height m | Diameter m | Volume m^3 | Weight $tons$ |
|--------------------|------------|--------------|--------------|---------------|
| Floating Structure | 52 | 110 | 44624,6913 | 10990.1543 |

For simulation purposes the 3D numerical wave tank was designed with length 1000 m , width 315 m and height 200 m . The water column height is 100 m . The density of the water is $\rho = 1025 \text{ kg/m}^3$.

The centre of gravity is on the bottom of the central floater of the structure 45 m below the water column surface. This is one of the significant elements of design for getting correct simulation results to ensure the stability of the structure. In the beginning, the simulations were taken place in still water without waves and mooring lines. The purpose of this kind of simulations was to obtain the stability of the

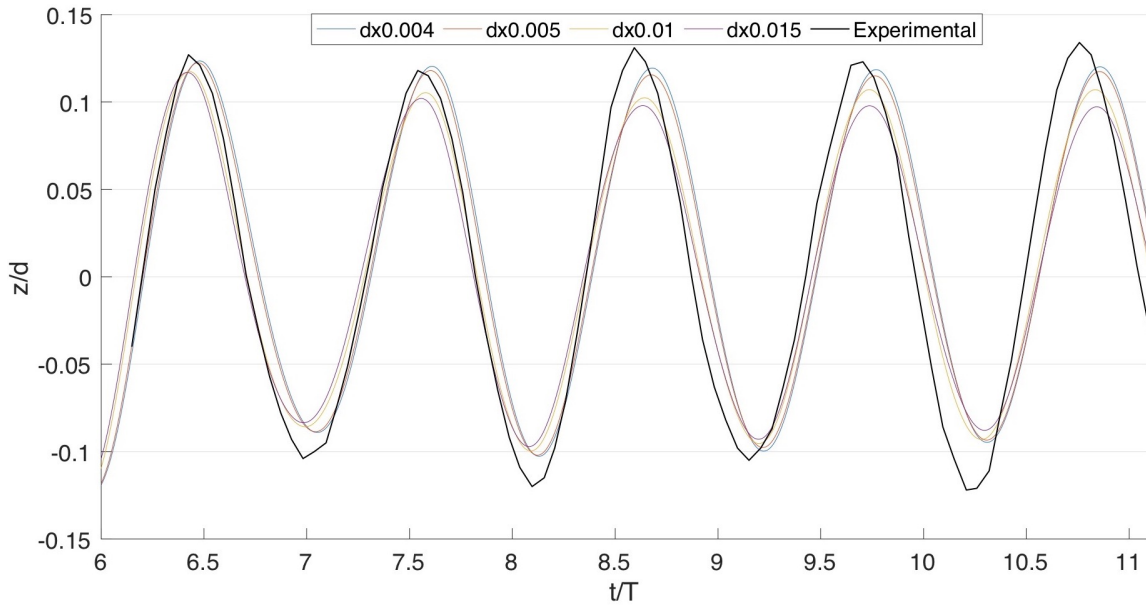


Figure 3.11: Floating Barge Heave Results with $H = 0.1 \text{ m}$

structure at the certain degree of submergence. The mesh size used in this case is $dx = 4.0 \text{ m}$. After obtaining certain results the waves and mooring lines for the floating structure was applied. The wave height is 0.06 m . The weight of mooring line is $m = 0.001 \text{ kg/m}$ and stiffness $k = 7 * 10^{12} \text{ N/m}$. The choice of these parameters is not accidental, as we remember from 3.1.1 the lowest impact to the heave motion of the floating cylinder was obtained with the lowest weight. However to ensure the reliability of the mooring system the stiffness parameter has been increased. Initially, the mooring lines length was taken longer as it is shown in the figure 3.21. However, under the action of wave forces, the floating structure was shifted by creating tension in mooring lines from one side and dangling state from another side as it is shown in figure 3.22.

After some period the centre of gravity of the structure was displaced to the side which led to the sinking of the structure. Proceeding from these obtained results the mooring system was installed under the strain. It should be noted that this kind of approach for mooring design is already in use in Oil and Gas industry platforms such as TLP (Tension Leg Platform) and FPSO (Floating Production Storage and Offloading). After several simulations the results of numerical data has shown improved stability of structure under the action of wave forces. The confirmation fo this fact can be found in the graphical representation of sway, heave and pitch motion of the structure 3.26, 3.27, 3.28.

This is a preliminary study. Further studies can be made on the basis of this case setup. For instance for increasing the redundancy of the mooring system and the

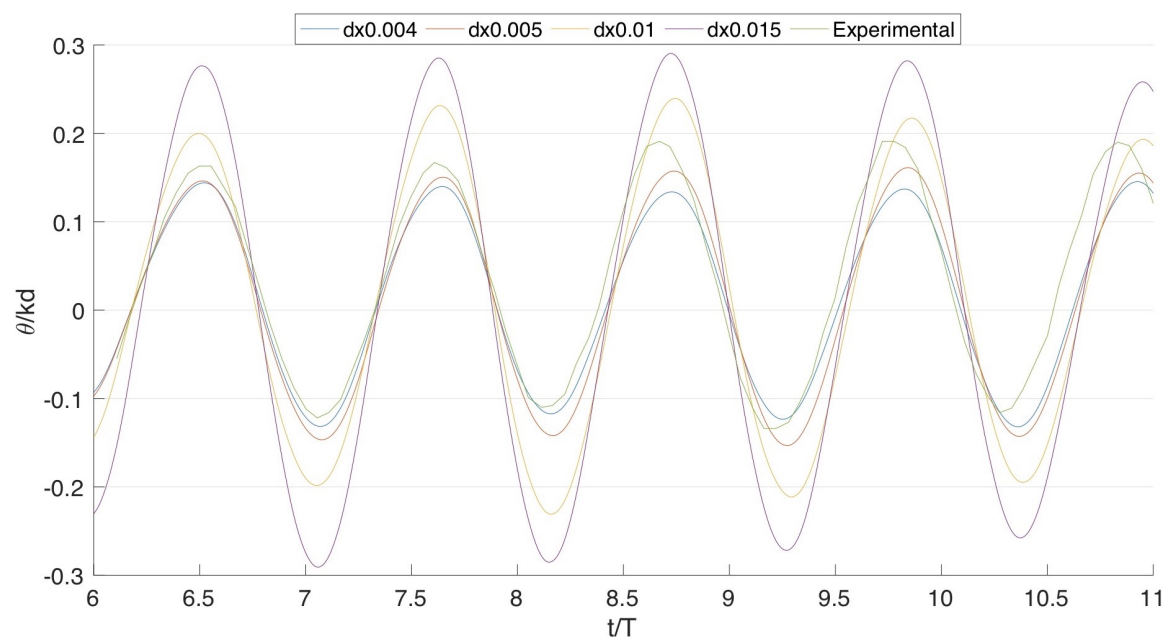


Figure 3.12: Floating Barge Pitch Results with $H = 0.1 m$

stability of the structure the number of mooring lines can be increased.

There are no any experimental data for this case for comparison with numerical data, however, further research can be done on the basis of this results for more detailed analysis.

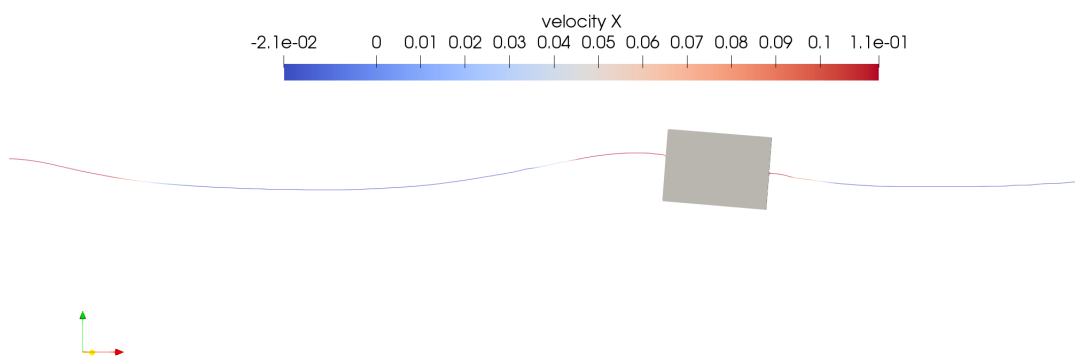


Figure 3.13: $t/T = 6.3$ with $H = 0.1 \text{ m}$

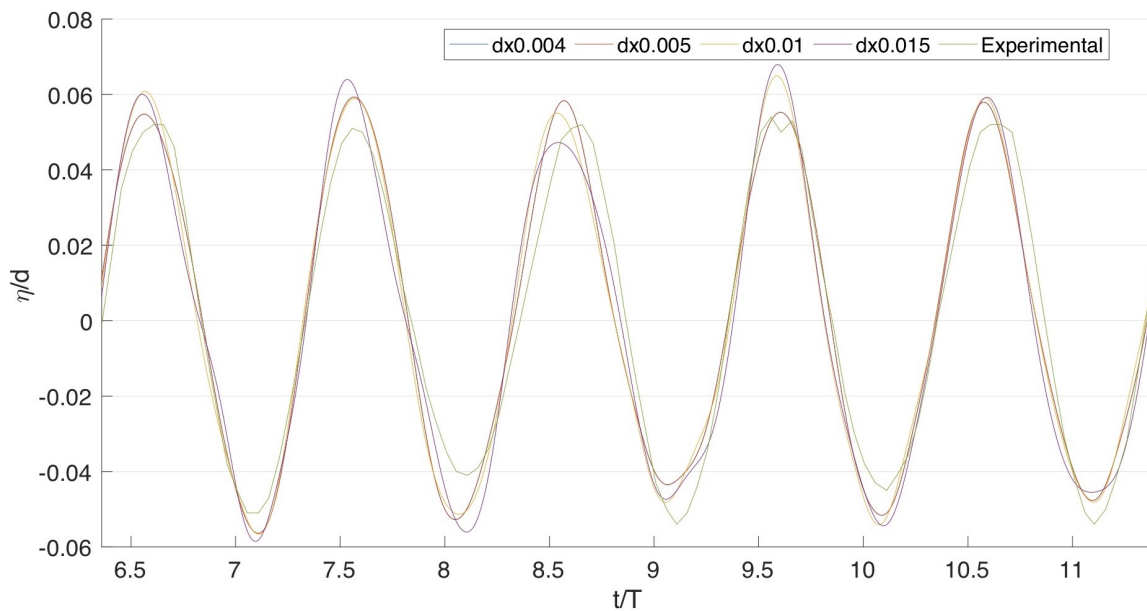


Figure 3.14: Floating Barge Wave Elevation with $H = 0.04 \text{ m}$

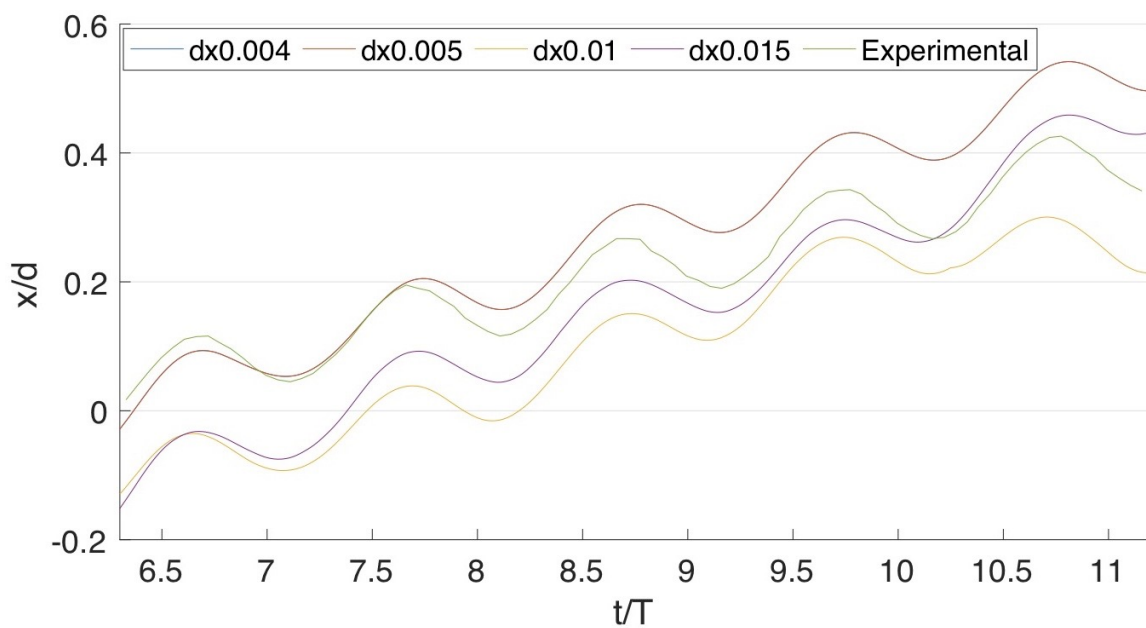


Figure 3.15: Floating Barge Sway Results with $H = 0.04\ m$

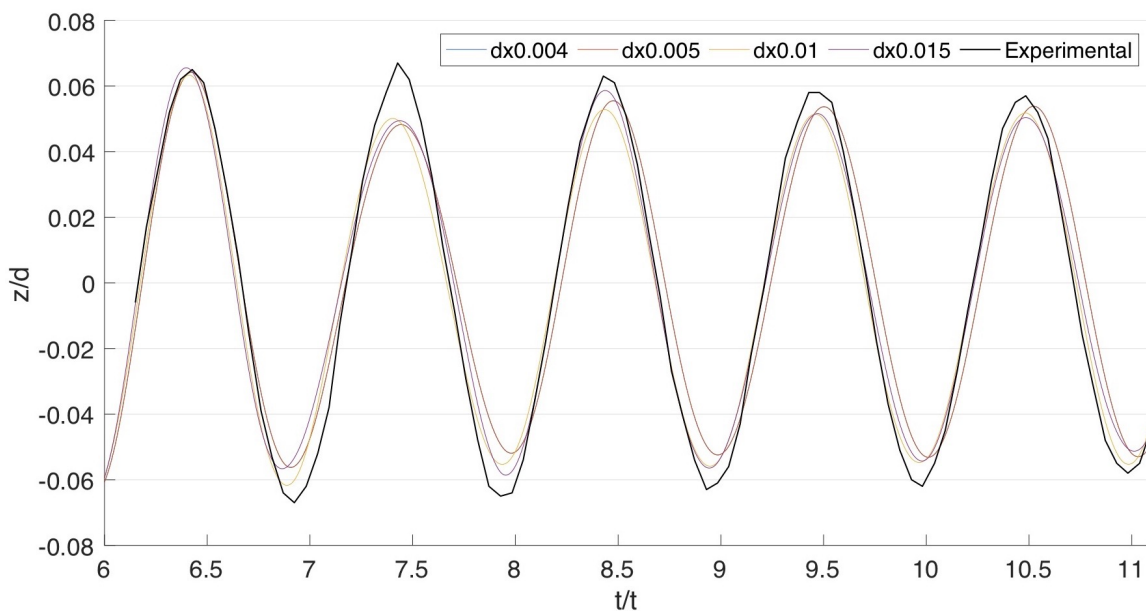


Figure 3.16: Floating Barge Heave Results with $H = 0.04\ m$

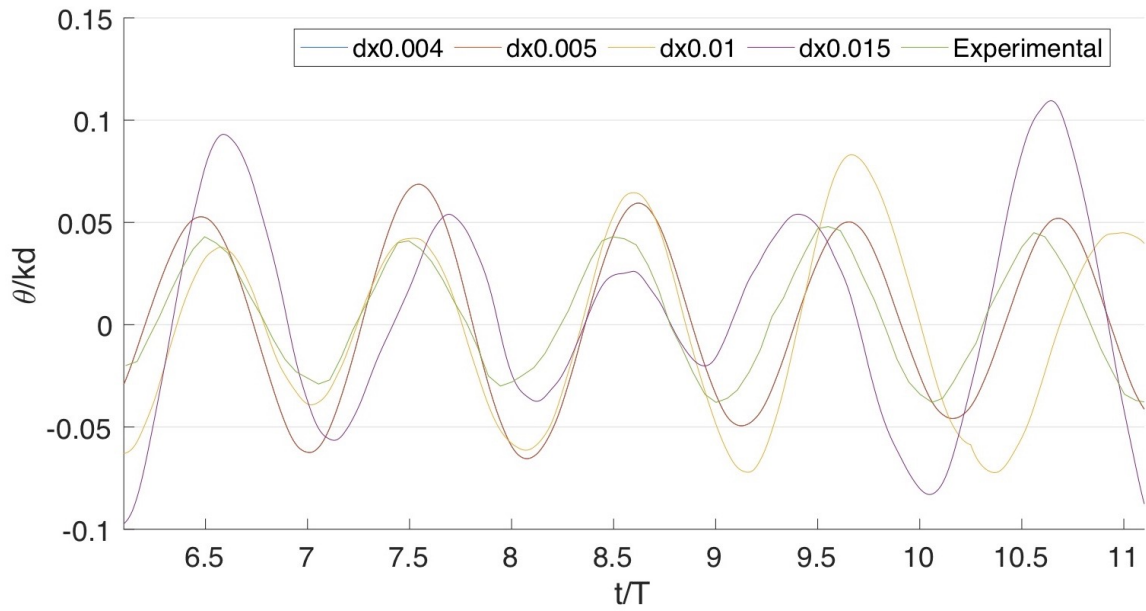


Figure 3.17: Floating Barge Pitch Results with $H = 0.04$ m

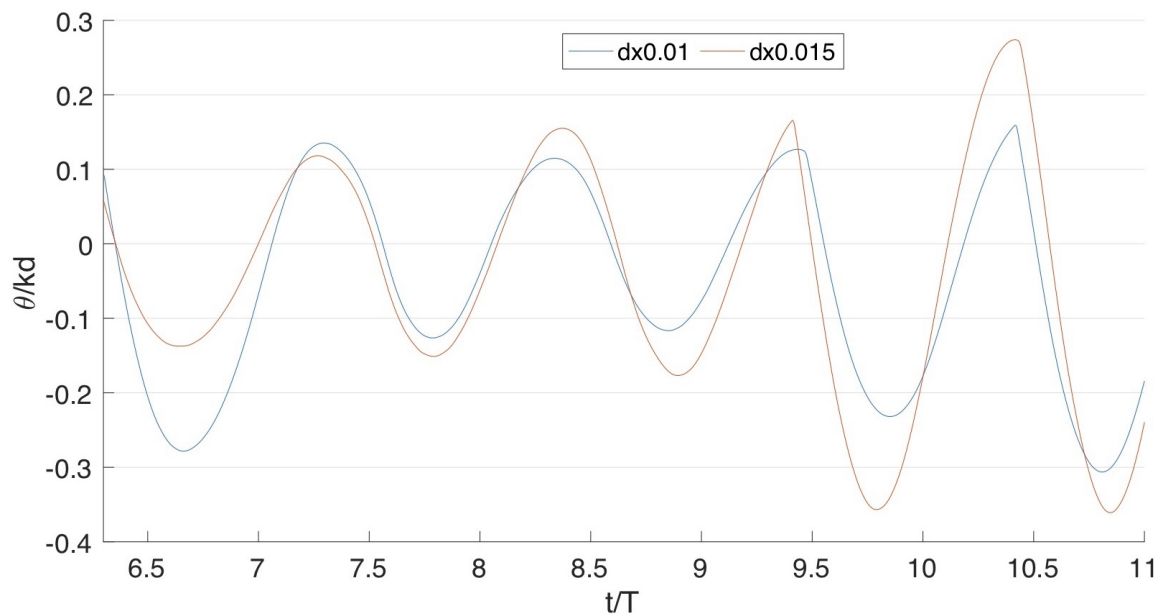


Figure 3.18: Mooring Applied Sway Results with $H = 0.1$ m

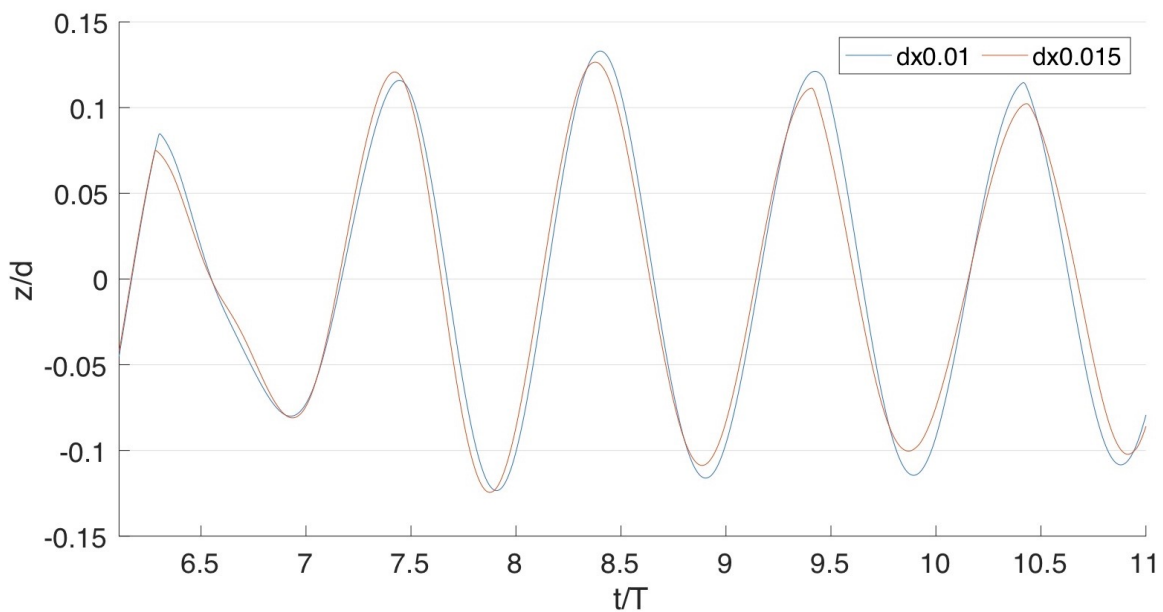


Figure 3.19: Mooring Applied Heave Results with $H = 0.1 \text{ m}$

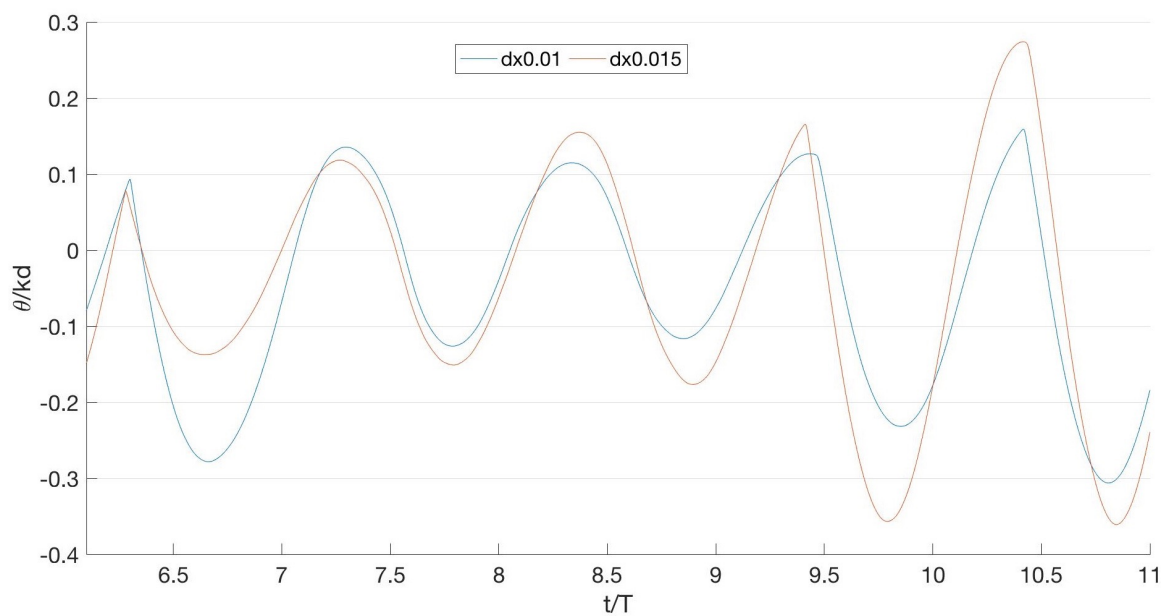


Figure 3.20: Mooring Applied Pitch Results with $H = 0.1 \text{ m}$

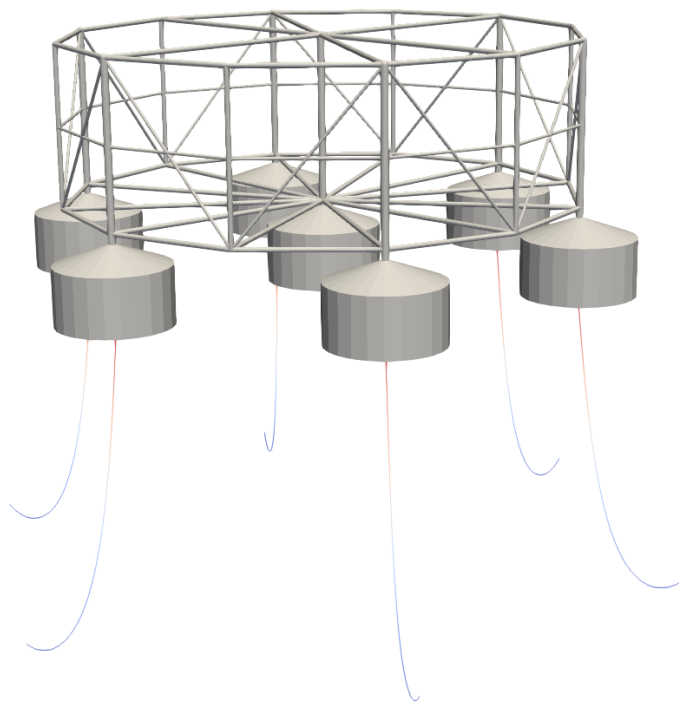


Figure 3.21: Initial State

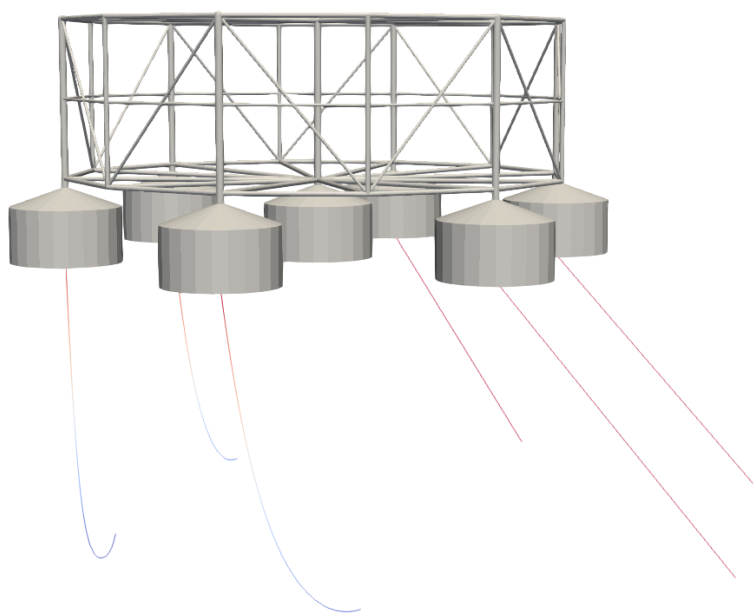


Figure 3.22: Under Action of Wave Forces

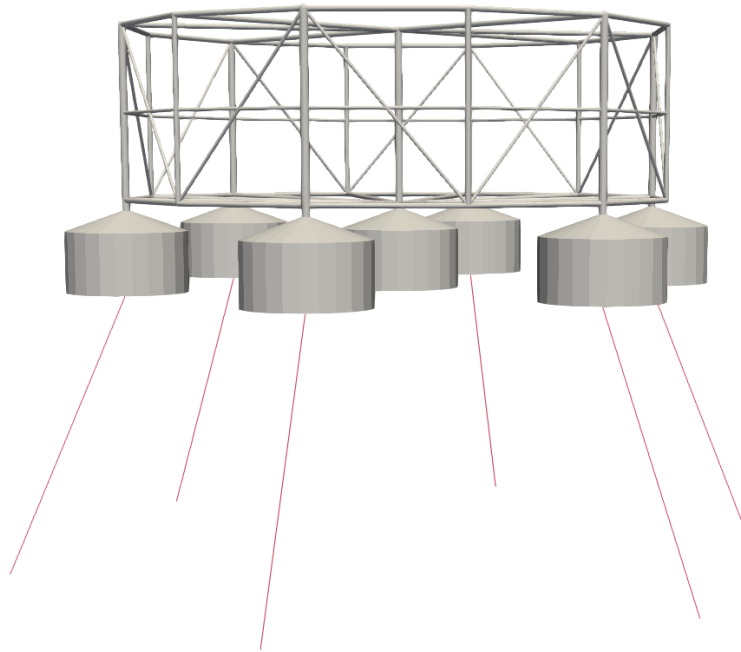


Figure 3.23: Strained Mooring Lines Design

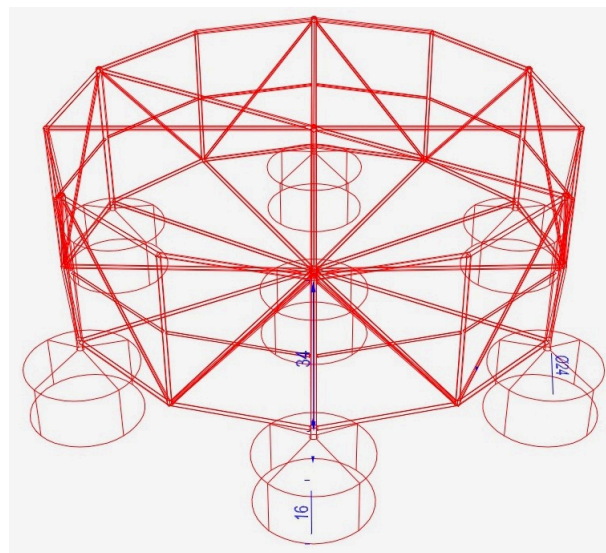


Figure 3.24: 3D Floating Structure

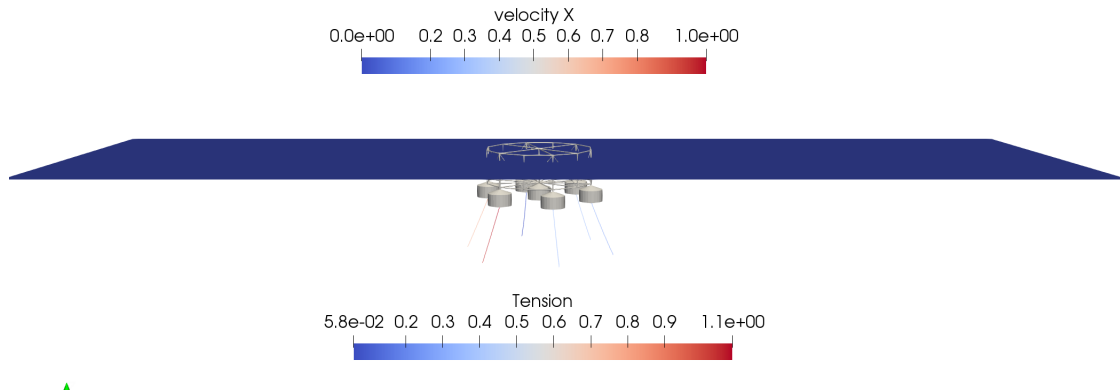


Figure 3.25: Three-dimensional structure motion with horizontal velocity x

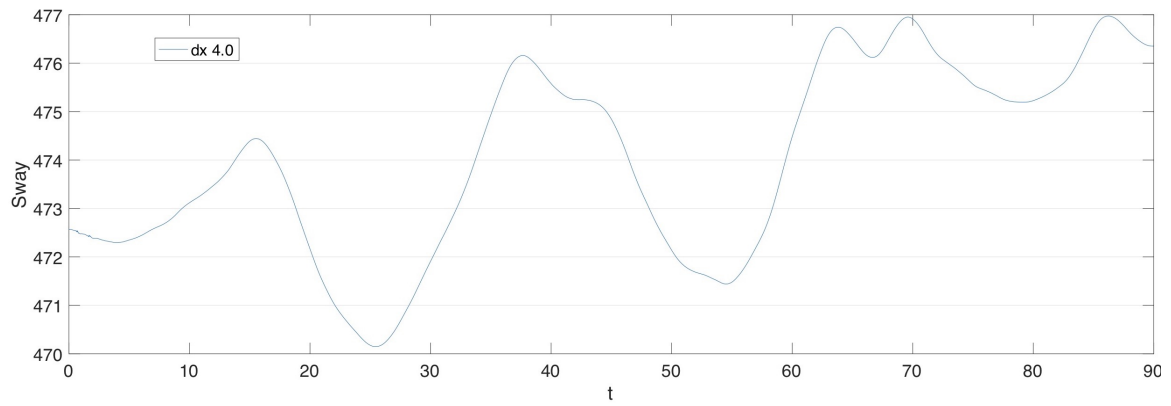


Figure 3.26: Sway Motion of 3D Floating Structure

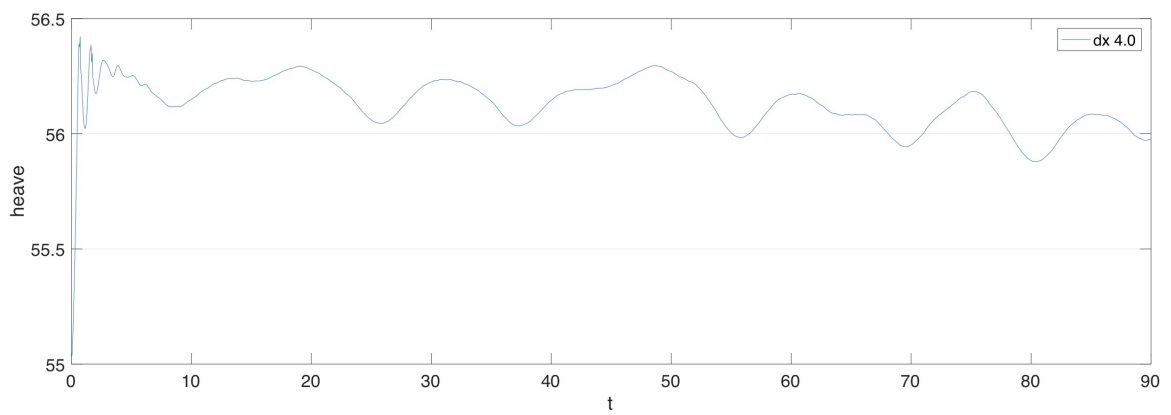


Figure 3.27: Heave Motion of 3D Floating Structure

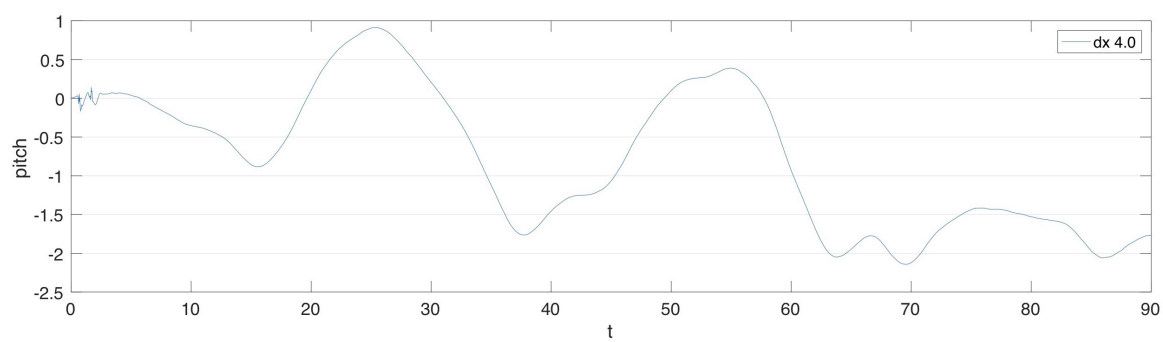


Figure 3.28: Pitch Motion of 3D Floating Structure

Chapter 4

Conclusions

The thesis was focused on the validation of numerical data for floating bodies as well as moored-floating bodies in waves using experimental data and a systematic investigation of the influence of different mooring systems on the motion of floating bodies. For this purpose in focus of the thesis work was concentrated on the motion of a free-floating body using the CFD model on REEF3D. After the validation of results obtained numerically for heave decay test for the cylinder with the finest mesh size, the goal was to apply this data on the free-floating barge with more complex 3DOF motion. In addition, different diameter cylinder sizes were analysed to observe and study changes in behaviour graphically. After that, the mooring system was employed for the stabilization of the cylinder at one point. Obtained results were also used in the 3DOF floating barge.

The floating barge 3DOF (sway, heave, pitch) motion was analysed and compared with experimental data. Numerically obtained results had convergence with experimental ones. In addition, mooring analyses were performed also for this case. Mooring system parameters used for 3DOF floating barge were the ones obtained and analysed from cylinder case.

The 6DOF motion of 3D structure has been analysed using the CFD model REEF3D. This was a preliminary study and further research can be made on the basis of this case setup. The case was studied with an application of a mooring system on the floating aquaculture structure. Mooring system used in this case was an imitation of already existing mooring systems used for TLP (Tension Leg Platform) and FPSO (Floating Production Storage and Offloading) platforms. CFD model is new generation tool in design and engineering challenges. The thesis task was to use CFD model to perform validation of the 6DOF algorithm and the mooring model. The obtained results were successful.

Bibliography

- [1] Alagan Chella M. Kamath A. Arntsen Ø.A. Ahmad N., Bihs H. Cfd modelling of arctic coastal erosion due to breaking waves. *International Journal of Offshore and Polar Engineering*, 2018.
- [2] Myrhaug D. Alagan Chella M, Bihs H. Characteristics and profile asymmetry properties of waves breaking over an impermeable submerged reef. *Coastal Engineering* 100:26–36., 2015.
- [3] Myrhaug D. Arntsen Ø.A. Alagan Chella M., Bihs H. Computation of wave impact pressures and kinematics during plunging breaking wave interaction with a vertical cylinder using cfd modelling. *36th International Conference on Ocean, Offshore & Arctic Engineering, Trondheim, Norway*, 2017.
- [4] Myrhaug D Muskulus M. Alagan Chella M, Bihs H. Breaking characteristics and geometric properties of spilling breakers over slopes. *Coastal Engineering* 95:4–19., 2015.
- [5] Alagan Chella M Arntsen ØA. Bihs H, Kamath A. Breaking-wave interaction with tandem cylinders under different impact scenarios. *Journal of Waterway, Port, Coastal, and Ocean Engineering*. DOI: 10.1061/(ASCE)WW.1943-5460.0000343, 2016.
- [6] Kamath A. Bihs H. A combined level set/ghost cell immersed boundary representation for simulations of floating bodies. *International Journal for Numerical Methods in Fluids, Vol. 83, Issue 12, pp. 905-916*, 2017.
- [7] Aggarwal A. Pakozdi C. Bihs T., Kamath A. Efficient wave modeling using non-hydrostatic pressure distribution and free surface tracking on fixed grids. *37th International Conference on Ocean, Offshore & Arctic Engineering, Madrid, Spain*, 2018.
- [8] Ping Dongb Hongjie Wen Bing Rena, Ming Hea. Nonlinear simulations of wave-induced motions of a freely floating body using wcsph method. *Applied Ocean Research*, 2015.

- [9] A. Chorin. Numerical solution of the navier-stokes equations. *Mathematics of Computation* 22 (104), 745–762., 1968.
- [10] P. A. Durbin. Limiters and wall treatments in applied turbulence modeling. *Fluid Dynamics Research.*, 2009.
- [11] Mayilvahanan Alagan Chella Ankit Aggarwal Øivind A. Arntsen Hans Bihs, Arun Kamath. A new level set numerical wave tank with improved density interpolation for complex wave hydrodynamics. *Computers and Fluids* 140:191–208, 2016.
- [12] Horia Ionescu. Six degrees of freedom. *Wikipedia the Free Encyclopedia*, 2010.
- [13] Arntsen ØA Kamath A, Bihs H. Numerical investigations of the hydrodynamics of an oscillating water column. *Ocean Engineering* 2015b; 102:40–50., 2015.
- [14] Bihs H Arntsen ØA. Kamath A, Alagan Chella M. Cfd investigations of wave interaction with a pair of large tandem cylinders. *Ocean Engineering* 108:738–748., 2015.
- [15] Bihs H. Martin T., Kamath A. Modelling and simulation of moored-floating structures using the tension-element-method. *37th International Conference on Ocean, Offshore & Arctic Engineering*,, 2018.
- [16] Alagan Chella M. Archetti R. Bihs H. Miquel A.M., Kamath A. Analysis of different methods for wave generation and absorption in a cfd-based numerical wave tank. *Journal of Marine Science and Engineering*, Vol. 6, Issue 2, Nr. 73,, 2018.
- [17] Fossen T.I. Guidance and control of ocean vehicles. *John Wiley & Sons: Chichester, England*,, 1994.
- [18] D. C. Wilcox. Turbulence modelling for cfd. *Journal of Fluid Mechanics.*, 1995.
- [19] Liang Yang. One-fluid formulation for fluid–structure interaction with free surface. *Computer Methods in Applied Mechanics and Engineering*, 2018.